PAPER

Check for updates

An unwanted guest in the electrochemical oxidation of high-voltage Li-ion battery electrolytes: the life of highly reactive protons†

Stefan Ilic, ‡[a] Milena Martins,‡[abf] Haoyu Liu,[c]
Pedro Farinazzo Bergamo Dias Martins,[ab] Dominik Haering,[a] Jingtian Yang,[c]
Toru Hatsukade,[a] Bostjan Genorio,[d] Stephen E. Weitzner,[e] Liwen F. Wan,[e]
Zhengcheng Zhang,[c] Justin G. Connell,[a] Baris Key,[c] Jordi Cabana *[a] and
Dusan Strmcnik *[ab]

Lithium-ion batteries (LIBs) are central to the urgent societal need to decarbonize both transportation and energy storage on the grid. Unfortunately, despite their attractive energy/power density, as well as high coulombic and energy efficiencies, further improvement of this technology – especially their durability – is desperately needed. To support these efforts, our study focuses on fundamental understanding of the decomposition pathways for LIB electrolytes at the cathode−electrolyte interface (CEI), as the nature of these reactions directly controls the extent to which cell capacity and voltage decays in these systems. In this study, we employ electrochemical methods, coupled with product analysis using NMR spectroscopy and mass spectrometry, to determine the decomposition mechanisms in both model and technologically relevant electrolytes. Remarkably, we discovered the electrochemical formation of protons with high chemical activity, comparable to known superacids, at potentials relevant to practical Li-ion batteries. Their reactivity toward every individual component of the CEI provides a unified thermochemical origin for a myriad of side reactions that are commonly associated with the electrochemical reaction. In particular, electrochemically generated protons react with intact EC molecules to form CO_2 and other short and long chain ethers. They also undergo an acid−base reaction with $LiPF_6$, to form the weaker acid HF, and with the cathode active material, leaching transition metals into the electrolyte. Collectively, the results of this study all point to the urgent need to either mitigate this proton formation or introduce benign harvesting additives *via* new electrolyte design strategies.

Broader context

Lithium-ion batteries are pivotal in the global transition to widespread electrification, by powering transportation and enhancing grid stability and resilience as renewable energy sources continue to penetrate. However, their widespread adoption faces challenges of durability and efficiency at high operating voltages needed to maximize energy density. The decomposition of battery electrolytes at such elevated voltages plays a central role in these challenges because it leads to capacity loss and reduced lifespan. This study identifies the formation of highly reactive protons, comparable to superacids, during solvent oxidation as a central driver of degradation in LIBs, triggering chemical cascades that compromise all battery components. These findings highlight a previously underexplored mechanism that directly impacts the longevity of LIBs and emphasize the urgent need for innovative electrolyte designs to mitigate proton generation and improve stability. The insights gained here will not only advance battery technology by enabling higher energy densities and longer lifespans in Li-ion devices but also inform emerging strategies for Na-ion systems that use similar electrolyte formulations. This work not only deepens our understanding of battery chemistry but also informs future strategies aimed at overcoming the energy-lifetime trade-off, paving the way for more reliable and durable energy storage solutions.

[a] *Materials Science Division, Argonne National Laboratory, Argonne, IL, USA. E-mail: jcabana@anl.gov*

[b] *National Institute of Chemistry, Ljubljana, Slovenia. E-mail: dusan.strmcnik@ki.si*

[c] *Chemical Sciences and Engineering, Argonne National Laboratory, Argonne, IL, USA*
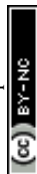
[d] *Faculty of Chemistry and Chemical Technology, University of Ljubljana, Ljubljana, Slovenia*

[e] *Laboratory for Energy Applications for the Future (LEAF) and Materials Science Division, Lawrence Livermore National Laboratory, Livermore, CA, USA*

[f] *Faculty of Chemistry and Chemical Engineering, University of Maribor, 2000 Maribor, Slovenia*

† Electronic supplementary information (ESI) available. See DOI: https://doi.org/10.1039/d5ee02403j

‡ These authors contributed equally to this work.

This journal is © The Royal Society of Chemistry 2025

Energy Environ. Sci., 2025, **18**, 8303–8312 | 8303

1. Introduction

In the quest for sustainable transportation solutions, lithium-ion batteries (LIBs) have emerged as a pivotal technology. LIBs have transformed the automotive industry, powering electric vehicles (EVs) and hybrid electric vehicles (HEVs). Their high energy density, long life span, and rapid charging capabilities have made them a viable alternative to traditional internal combustion engines. With advancements in battery technology, EVs have become more accessible and affordable, promoting a greener and cleaner transportation ecosystem. Moreover, the integration of renewable energy sources with LIBs enables the storage and distribution of clean electricity, paving the way for a transportation future powered by renewable sources.

However, despite their attractive energy and power density, high coulombic and energy efficiencies, and long lifespan, further improvement of this technology is urgently needed to meet the stringent metrics that are required in order to unlock EVs as a viable mass-market transportation solution.[1–3] In particular, consumer expectations of vehicle autonomy, safety and cost of ownership demand simultaneous leaps in energy density and lifetime. Given that cathodes currently limit the energy stored in Li-ion batteries,[4] achieving this goal requires approaching the theoretical capacity of modern layered oxides, $Li_xNi_yMn_zCo_{1-y-z}O_2$ (NMC), which, by virtue of their fundamental mechanism of operation, will inevitably involve a parallel, and welcome, increase in the operating voltage of the battery. However, operation at ever increasing voltages is hindered by the intrinsic stability limits of the available electrolytes[5–7] and the existence of a variety of competing processes involving the cathodes.[8,9] The result is a tangle of reactions that lead to detrimental gaseous, liquid and solid products, and an observable trade-off between energy and lifespan.

Unfortunately, a fundamental understanding of the degradation phenomenon that untangles the complexity of deleterious processes is lacking, even for existing commercial cathode materials and electrolytes, and lags far behind the push to develop novel cathode chemistries, solvents, additives, and electrolyte salts. The result is that this development is informed by simplified pictures and often based on empirical optimization. Because of the complexity of degradation processes at the cathode–electrolyte interface (CEI), there is an ongoing debate over which set of processes are primarily responsible for the diminishing LIB performance. This lack of understanding has created a significant hurdle for the implementation of targeted remedies that can truly bypass problematic degradation processes. The ability to isolate these key factors is complicated by the fact that a confluence of processes has been identified to occur when capacity fades. For instance, oxidation of the electrolyte at high potential, assisted by conducting carbon additives[10,11] and the oxide cathode,[12,13] is accompanied by the formation of passivating layers,[14,15] reconstruction of the electrode surface[16–18] and transition metal dissolution.[19–21] There is also the evidence of crossover of gas and liquid/dissolved products of these reactions from the cathode and

the anode,[22,23] propagating degradation beyond the CEI. Although there is ample evidence that all these processes do indeed occur, far less is known about their mechanistic hierarchy, namely how, when, where and why these reactions occur and to what extent they cause performance loss of LIBs rather than simply correlate with it.
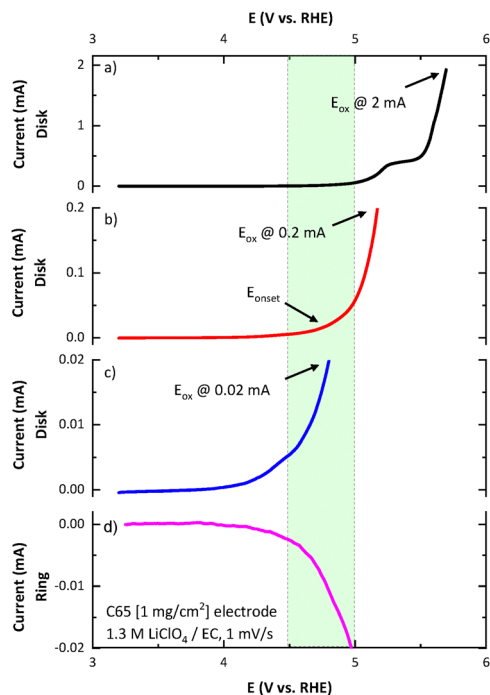
In this study, we identify the formation of protons during the electrochemical oxidation of typical Li-ion battery electrolytes as a key driver of the decomposition of each individual component of the CEI – the solvent, salt, and cathode active material. Using inert electrodes such as single crystal Pt(111), and combined electroanalysis and NMR spectroscopy, we quantify the amount of protons formed throughout the oxidation of the electrolyte based on ethylene carbonate (EC), arguably the most common solvent in LIB electrolytes. We show that proton formation already has a measurable impact on faradaic efficiency at potentials >4 V. We further demonstrate their uniquely high chemical activity, comparable to known super-acids, and how it causes them to play a major catalytic role in chemical cascades that involve other degradation reactions of EC, quantitative displacement of HF from PF_6^- in the electrolyte, and cation leaching from oxide cathode materials to form dissolved transition metal cations and water. Overall, our work identifies that remediating the anodic production of protons is a priority to design electrolytes with transformative stability that potentially breaks the energy density-lifetime trade-off of current Li-ion technology.

2. Results and discussion

2.1 Establishing the potential window to probe electrolyte stability

In the available literature, it is common to report oxidation potential, E_{ox}, or onset potential, E_{onset}, as the measure of anodic stability of a particular solvent or electrolyte. While there have been reports on the computation evaluation of thermodynamic E_{ox},[24,25] the true value can only be obtained when the decomposition mechanism is known. Given that different reports predict different mechanisms such as ring-opening reactions,[26–31] oxidative dehydrogenation,[32,33] or reactions involving cathode oxygen,[34,35] the experimental validation becomes indispensable. Furthermore, we point out that, for an irreversible electrochemical process, experimental determination of both E_{onset} and E_{ox} is rather arbitrary and therefore cannot be accurately compared with the values calculated from thermodynamically derived computations. A simple demonstration of the problem is depicted in Fig. 1a–c, where we show the same polarization curve on 3 different current scales for the decomposition of 1.3 M $LiClO_4$ in EC on the Super-C65 carbon electrode, a common conductive additive in Li-ion batteries, probed in a rotating ring-disk electrode (RRDE) setup (see Experimental methods for details). Clearly, establishing either E_{ox} or E_{onset} is highly challenging in this experiment, as they both depend on the choice of the current value that is determined to indicate the existence of the reaction of interest. For

8304 | Energy Environ. Sci., 2025, 18, 8303–8312

This journal is © The Royal Society of Chemistry 2025

Fig. 1 Electro-oxidation of the 1.3 M LiClO$_4$/EC electrolyte on C65 carbon, deposited on a glassy carbon disk in a RRDE setup with a Pt ring. The current *vs.* potential response on the disk from the same experiment is shown on three different current scales, up to (a) 2 mA, (b) 0.2 mA and (c) 0.02 mA. The ring current (d) is measured at 2.8 V *vs.* Li/Li$^+$ and is directly connected to the formation of protons, created during oxidation of the solvent. Fig. S1 shows the expanded ring current window (ESI†). Green shading denotes potential ranges with pronounced proton formation.

instance, as the current threshold is tightened, E_{onset} shifts to lower potentials. Since this kind of measurement is often used to screen electrolytes for their anodic stability, the arbitrariness of this observation points to a critical need to build a consensus within the community for the relevant value(s) of i_{ox} that enable a meaningful assignment of E_{ox}. A common framework for comparing electrolyte stability obtained by different laboratories is needed, which reports and discusses the current densities at different potentials that are relevant for a particular application.

Solvent oxidation potentials should be determined at sufficiently high current densities to ensure that the response is coming from the most abundant species in the system. We believe that 5 mA cm^{-2} or higher is sufficient to achieve this. While, in principle, the E_{ox} values can be collected on any electrode, doing so on real composite electrodes that contain conducting carbon and cathode materials can be quite challenging due to problems with electrochemically active surface area (ECSA) determination. We therefore suggest that for the studies focusing exclusively on solvent stability, flat and inert electrodes should be used, where the geometric surface area of the electrode can be used to extract the current densities. The E_{ox} can then be determined either by potentiodynamic (CV and LSV) or galvanostatic (CP) measurements. However, when we are interested in the solvent decomposition on the high voltage

Li-ion cathodes under relevant conditions, we should monitor the solvent oxidation currents in the 4.5–5.0 V range. Unfortunately, this approach becomes problematic when measuring actual battery composite electrodes, because the signal from the active material is much larger than the parasitic current due to electrolyte decomposition. Therefore, measuring the current associated with the generation of species linked exclusively to the oxidation of the solvent is a far better option. Below, we discuss such an approach, using the RRDE method for proton detection.
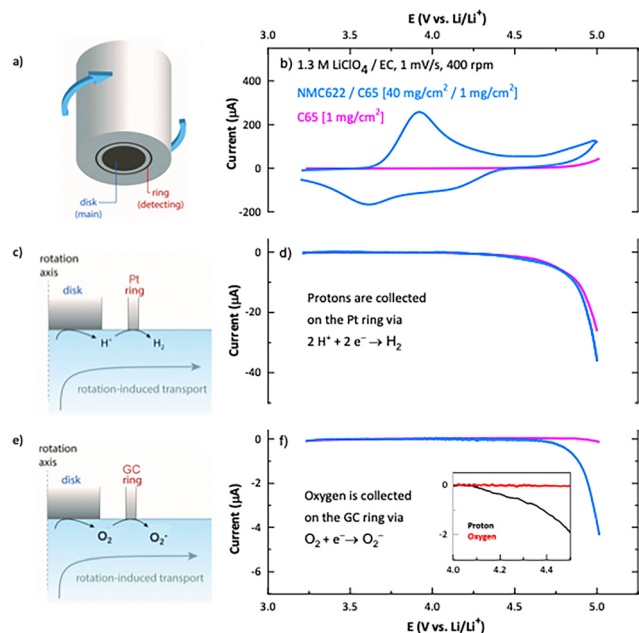
2.2 Proton generation

The mechanism of electrochemical oxidation of organic compounds often involves proton transfer.[36–38] It is reasonable to assume that the electro-oxidation of the LIB solvents would follow a similar mechanism. We recently reported an electro-analytical protocol of amperometric detection of these protons in real time using an rotating-ring disk electrode (RRDE, Fig. 1d and 2a–d).[39] Indeed, Fig. 1d shows that the current response on a ring that is set to track the production of protons follows the current signal of the disk (the Pt ring is biased at just below the standard reduction potential for the H$^+$/H$_2$ conversion), confirming that electrolyte oxidation does in fact occur already at potentials below 4 V *vs.* Li/Li$^+$, well within the normal cycling range of conventional NMC based cathodes. Further confirmation of proton formation is provided *via ex situ* nuclear magnetic resonance (NMR) experiments discussed below. We propose that this framework for detecting protons generated from solvent decomposition provides a means to standardize the screening of electrolytes according to their anodic stability. However, we note that for the composite electrolytes consisting of several solvents, additives and impurities, this method will inevitably detect protons from the least oxidatively stable species.

The RRDE can also deconvolute the decomposition of electrolytes from other simultaneous electrochemical processes, such as charging and discharging of the cathode material, carbon oxidation and anion intercalation, or lithium carbonate decomposition. The power of the method was demonstrated by comparing a composite cathode made of LiNi$_{0.6}$Mn$_{0.2}$Co$_{0.2}$O$_2$ (NMC622) and C65 with a pure C65 electrode (Fig. 2b). Several observations are noteworthy here: (i) we can deconvolute the electrochemical solvent decomposition easily from the charge/discharge process; (ii) the charge passed for solvent decomposition is roughly 0.5% of the total up to 5 V in the first cycle; (iii) the amount of produced protons is roughly the same on electrodes with and without the active material. This latter observation suggests that most of the electrochemical solvent decomposition occurs on the carbon material, which is likely the consequence of its massively higher surface area compared with NMC, and not some intrinsic catalytic properties of the active material.

As shown in the study by Grimaud *et al.*, the RRDE technique can also be employed to amperometrically detect oxygen release from NMC materials,[40] which can cause chemical oxidation of the solvent. In a separate experiment, we employed

This journal is © The Royal Society of Chemistry 2025

Energy Environ. Sci., 2025, **18**, 8303–8312 | **8305**

Fig. 2 Electrochemical detection of parasitic processes during the charge–discharge of the NMC622/C65 composite electrode (blue) and the inert C65 electrode (pink) with a RRDE setup (a). The total current is measured on the disk (b), while the portion of the current contributing to solvent oxidation is detected on the Pt ring at 2.8 V vs. Li/Li⁺ through the reduction of protons (c) and (d). In a separate experiment, the oxygen release from the cathode material is detected on a GC ring at 1.8 V vs. Li/Li⁺ through reduction to superoxide (e) and (f). The inset shows the difference in the proton and oxygen formation at potentials relevant for cathode cycling.

this method to quantify O_2 formation (Fig. 2e) using a glassy carbon ring to differentiate oxygen formation from proton reduction. As shown in Fig. 2f, the electrochemical oxidation leads to the O_2 formation on the NMC622/C65 electrode. However, the onset potentials for these processes are much more positive than proton formation. Indeed, in the typical potential range where current cathodes are cycled (~ 4.3 V vs. Li/Li⁺), we observe only proton formation (Fig. 2f, inset). Nonetheless, it is important to note that the electrochemically generated oxygen will have a much more prominent role in the solvent degradation as the upper cutoff potentials are raised, although proton generation will also increase concurrently.[41–43]

2.3 Impact of protons on solvent decomposition

After establishing the extent of LiClO₄/EC electro-oxidation at relevant potentials, we move to investigate the impact of the created protons on the individual components of the cathode/electrolyte interface. We again employ 1.3 M LiClO₄/EC as a model electrolyte to avoid confounding reactions, since protons should not induce decomposition of LiClO₄, unlike the conventional electrolyte salt, LiPF₆, as we reveal below. We performed a series of experiments where 1.5–45 coulombs of charges were passed through the LiClO₄/EC electrolyte galvanostatically at 2–10 mA output current using a Pt(111) electrode

at 900 rpm rotation rate (the output potentials are available in Fig. S2, ESI†). This amount of charge generates proton concentrations in the range of 3–67 mM, comparable to the concentration of protons one charging cycle at 0.1–1 mV s⁻¹ in Fig. 2d, would create in a coin cell battery. The inert Pt(111) electrode was utilized to isolate the solvent decomposition from concurrent electrode activity (e.g., from carbon oxidation and NMC charging). Proton evolution was tracked by ¹H NMR spectroscopy (Fig. 3a). The proton concentration was calculated based on the peak area and calibrated by normalizing from the peak area of an external standard (10 mM VC in the pristine LiClO₄/EC electrolyte). The signals appeared at chemical shifts around 18 ppm, significantly downfield shifted compared to typical organic acids (11–12 ppm).[44] In fact, the exceptional deshielding observed for these electrogenerated protons is the reminiscent of the NMR shifts observed for many known superacids,[45] such as triflic acid (13.5 ppm),[46] fluorosulfuric acid (14.5 ppm),[47] fluoroantimonic acid (16 ppm)[48] and carborane acid (20.4 ppm).[49] This stark comparison anticipates that the electrogenerated protons will be aggressive acids. The ¹H peak persisted after a whole week of storage of the decomposed electrolyte, but it shifted slightly and significantly broadened from only 2 Hz to 35 Hz, indicating an evolving and much less homogeneous local chemical environment. Nonetheless, the proton concentration remained fairly constant over the course of 7 days, indicating that they were not being consumed to a significant extent.

Further analysis of ¹H and ¹³C NMR spectra (Fig. 3b and Fig. S3, ESI†) revealed that vinylene carbonate (VC) and reactive protons are formed as the main products of the electrochemical oxidation of EC (see day 1 in Fig. 3b). VC has been previously reported as a product, but often as not the main product.[32,33,35] The formation of VC via electrochemical oxidation of EC was also probed using grand canonical DFT calculations. The detailed description of the computational method can be found in the ESI.† As shown in Fig. S6 and S7 (ESI†), the electrochemical transformation of EC to VC is found to be thermodynamically favourable at potentials greater than 3 V vs. Li/Li⁺. When considering the role of surface interactions, under all conditions considered, the desorption of VC from Pt surfaces may be a rate determining step in the oxidation process, requiring significant overpotential to overcome. Based on the experimental and theoretical results, we have concluded that the electrochemical reaction of EC oxidation proceeds according to eqn (1):

$$EC_{(l)} \rightarrow VC_{(l)} + 2H^+_{(sol)} + 2e^- \tag{1}$$
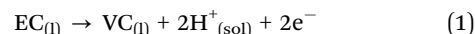
Several side products and intermediates were found to dynamically evolve with storage time. A comprehensive analysis of their identity and behaviour is beyond the scope of this work, and it will be the subject of a separate detailed study to be published elsewhere. For the purposes of this discussion, we focus on products that have been proposed in the literature as resulting from the electrochemical decomposition of the electrolyte under applied potential.[27,32,33,35,42,50–60]
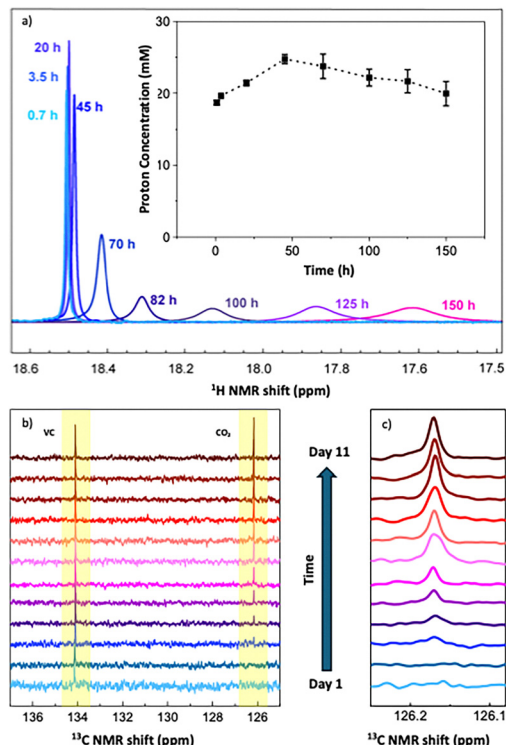
Fig. 3 Selected NMR spectra after electrochemical oxidation of the 1.3 M $LiClO_4$/EC electrolyte: (a) the ^1H shift of protons electrogenerated from a $LiClO_4$/EC electrolyte as a function of time after electrochemical oxidation. The inset shows the proton concentration calculated based on the peak area and calibrated with an external standard (10 mM VC). Standard deviation for each point is shown as an error bar. (b) ^{13}C NMR spectra (126–134 ppm) in the $LiClO_4$ EC electrolyte recorded each day from day 1 to day 11 highlighting VC and CO_2 generation. (c) Zoom-in of the CO_2 ^{13}C NMR signal change with time.

We start by highlighting the absence of CO_2 in the NMR spectrum collected shortly after passing 45 coulombs of charge (Fig. 3c). Instead, we observed significant CO_2 formation over the course of several days, according to both ^{13}C NMR and GC-MS analyses (Fig. 3c and Fig. S4, ESI†). This observation suggests that the most CO_2, which has been assigned as a major product of electrochemical EC oxidation *via* ring opening in the literature,[41,61–63] is instead produced by a chemical cascade that follows the electrochemical reaction. To resolve the discrepancy in the proposed origin of CO_2 between our data and the literature, we also performed deliberate electrolyte oxidations at several scan rates in an online electrochemical mass spectrometry (OEMS) setup (Fig. S5, ESI†). We found that the passed anodic charge approaches the amount of CO_2 generated at scan rates close to the ones reported in the literature (*i.e.* long-time scale),[41,61–63] so one could be misled into concluding that the observed CO_2 is produced electrochemically. However, as the scan rates increase (*i.e.* shorter timescales), it becomes clear that the majority of the charge does not go towards the production of CO_2. In fact, CO_2 production decreases with higher scan rates, *i.e.*, in shorter experiments, to the point of being barely detectable.

In addition, other C_1 or C_2 products, such as formaldehyde, acetaldehyde, ethanol, *etc.*, proposed to originate from ring

opening and fragmentation[26,33,60,64,65] were not detected by NMR, GC-MS or OEMS immediately after electrolyte oxidation. Instead, we observed several products forming in the days following electro-oxidation, including 1,4-dioxane and 2-methyl-1,3-dioxolane as well as the CO_2 in the electrolyte headspace on day 2–10 following electro-oxidation, as revealed by GC-MS results in Fig. 4a. This result highlights that previously reported decomposition products originate from a chemical cascade, rather than from the direct electrochemical oxidation of the solvent.

The appearance of ether functionalities over the course of several days is also confirmed by NMR (Fig. S8, ESI†). Comparing the NMR spectra of the $LiClO_4$/EC electrolyte in its pristine state and on day 2 and day 9 after oxidation, we observe the appearance of a ^1H peak at 3.69 ppm and a ^{13}C peak at 68.3 ppm, the main NMR signatures for the $-CH_2CH_2O-$ unit. In agreement with GC-MS data, such ether formation was first observed on day 2 in a very small amount, which kept evolving in the following week, accompanied by an obvious colour change from pale yellow to brown (Fig. 4b). The unoxidized sample showed no colour change during the same timeframe (Fig. S9, ESI†). We were also able to detect a small amount of oxirane (Fig. 4c) in a separate GC-MS analysis performed on a different column using a dynamic headspace sampler (see Experimental methods for details). As with CO_2, these products form continuously without any sign of significantly slowing down over the course of the measurement. These results suggest that ether compounds, also reported in the literature
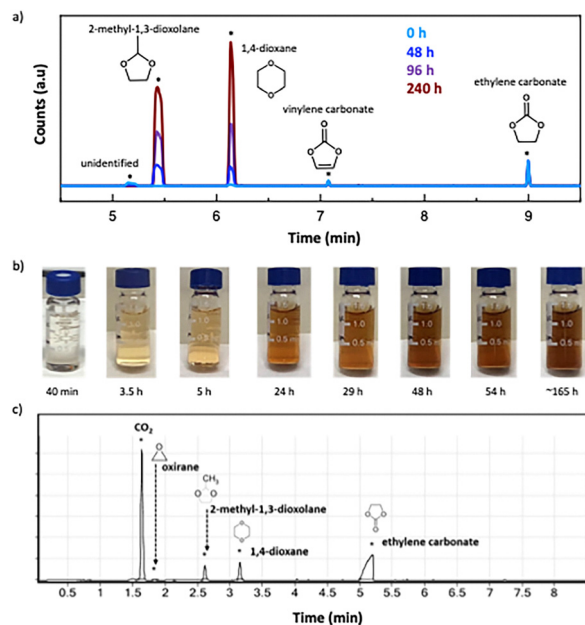

Fig. 4 (a) Detection of decomposition products with GC-MS using a Rxi-624Sil MS capillary column. 100 μL of the sample headspace was injected directly onto the column at various times elapsed after passing 45C of the charge through the electrolyte. (b) A change in colour was observed with time after the electrolyte was oxidized with 45C. (c) Detection of decomposition products with GC-MS. The headspace of a sample after passing 1.5C of the anodic charge through the electrolyte was analysed on day 7 using a dynamic headspace sampler and a DB-5MS capillary column.
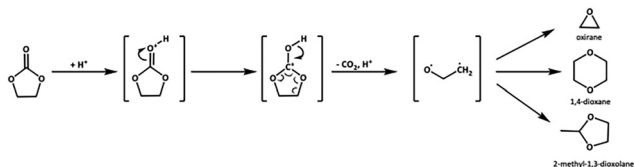
This journal is © The Royal Society of Chemistry 2025

Energy Environ. Sci., 2025, **18**, 8303–8312 | **8307**

Fig. 5 Proposed reaction scheme for H^+-catalyzed decomposition of EC. The reaction branches out after the formation of CO_2 and $^\bullet O-CH_2-CH_2^\bullet$ moieties from the ring opening process, to form a series of ether-based molecules and polymers. The scheme shows molecules detected in our experiments only.

as products of the electrochemical oxidation of propylene carbonate,[62] are likely rather formed *via* a chemical reaction pathway initiated by electrochemically generated protons.

To explain the combination of results presented so far, we propose a chemical decomposition mechanism of EC that follows the electrochemical process (Fig. 5). H^+ from the electrochemical reaction plays the role of a catalyst in this chemical cascade, and, hence, are not consumed, as its concentration remained constant over several days (Fig. 3a, inset). They initiate the ring opening of pristine EC remaining after the anodic process, resulting in the release of CO_2 and formation of $-O-CH_2-CH_2-$ moieties, and the common building block of all three molecules we were able to detect. It is plausible that ethers with a higher number of "base units" (>2) probably form but were not detected by GC-MS in the headspace, due to their low vapor pressure. PEO-like polymer chains, also reported in the literature, can also display almost identical $^1H/^{13}C$ shifts as the ones observed here.[66]

2.4 Impact of protons on the electrolyte salt decomposition

As demonstrated above, the $LiClO_4$/EC electrolyte system made it possible to track the chemical cascades of solvent decomposition that arises from protons generated in the initial anodic process at high potential. However, a more realistic LIB electrolyte contains $LiPF_6$ as the primary salt. In this case, a reasonable hypothesis would be that the electrogenerated protons will react with the PF_6^- anions to produce HF, a much weaker acid (based on NMR shifts)[60] known to form at cathode–electrolyte interfaces.[67] In Fig. 6, we show the evolution of the concentration of HF in the $LiPF_6$/EC electrolyte after the introduction of 3 mM protons through electrochemical oxidation of EC, tracked by a F^- ion selective electrode.[68] There was a quantitative conversion of H^+ to HF from PF_6^- through reaction (2).

$$H^+ + PF_6^- \rightarrow HF + PF_5 \qquad (2)$$

Hence, we conclude that PF_6^- anions serve as a natural buffer that mitigates the extreme acidity of the electrolyte after oxidation, at the cost of forming a species, HF, which is known to trigger other degradation processes in Li-ion batteries.[69,70] Importantly, the quantitative reaction happens on the timescale of hours (Fig. 6). Thus, locally electrogenerated protons have ample time to interact with other components of the cathode or the electrolyte, including the solvent, before getting completely consumed *via* HF displacement.
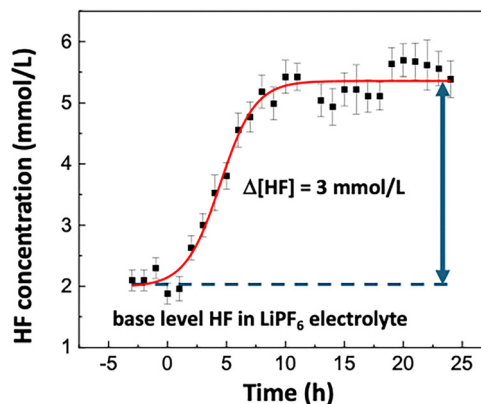

Fig. 6 Quantitative formation of HF in 1.3 M $LiPF_6$/EC after accumulating 1.5C of the anodic charge, which corresponds to the creation of 3 mM of protons. A baseline concentration of HF was established at 1 h time intervals (see data before $t = 0$) prior to introducing protons *via* anodic currents. The baseline concentration of HF in the electrolyte was 2.2 mM. The final concentration of the HF was measured at around 5.2 mM. The standard deviation for each point is shown as an error bar.

2.5 Impact on the cathode decomposition

Next, we investigated the interactions of the electrogenerated protons with one of the leading cathode materials for Li-ion batteries, $LiNi_{0.6}Mn_{0.2}Co_{0.2}O_2$ (NMC622). Again, 3 mM of protons were introduced *via* electrochemical oxidation of 5 mL of 1.3 M $LiClO_4$ in EC, in which 30 mg of NMC622 were immersed. The concentration of transition metals in the electrolyte was monitored using ICP-MS at periodic intervals for up to 10 hours (Fig. 7). Very small rates of dissolution ($\sim$100–200 ppb) were measured in this time interval as long as the active material initially had a native Li_2CO_3 layer (Fig. 7a and Fig. S10, ESI†), which is commonly present after prolonged storage or surface treatments.[71–73] Li_2CO_3 can react with protons to release CO_2 *via* reaction (3):

$$Li_2CO_3 + 2H^+ \rightarrow 2Li^+ + CO_2 + H_2O \qquad (3)$$
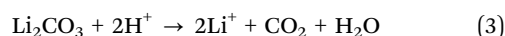
which effectively neutralizes them prior to the reaction with the pristine surface of the active oxide exposed after removing the carbonate. This mechanism provides another explanation for the detection of CO_2 during electrode charging, as electrogenerated H^+ can proceed to chemically digest native Li_2CO_3 layers on the oxide cathode. Up to two orders of magnitude, higher dissolution was observed when the NMC powders were washed prior to the experiment to effectively remove Li_2CO_3 (Fig. 7b). Dissolution of all three transition metals from the cathode was found during the probing time, with concentrations reaching as high as 20 ppm. The dissolution of native NMC622 with the oxidized 1.3 M $LiClO_4$/EC in Fig. 7b follows the reaction (4):

$$LiNi_{0.6}Mn_{0.2}Co_{0.2}O_2 + 4H^+ \rightarrow Li^+ + 0.6Ni^{2+/3+} + 0.2Mn^{4+}$$
$$+ 0.2Co^{3+} + 2H_2O \qquad (4)$$
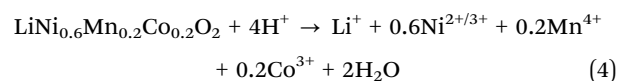
The amount of transition metals in the solution after 10 h from ICP-MS measurements suggests almost quantitative

8308 | *Energy Environ. Sci.*, 2025, **18**, 8303–8312

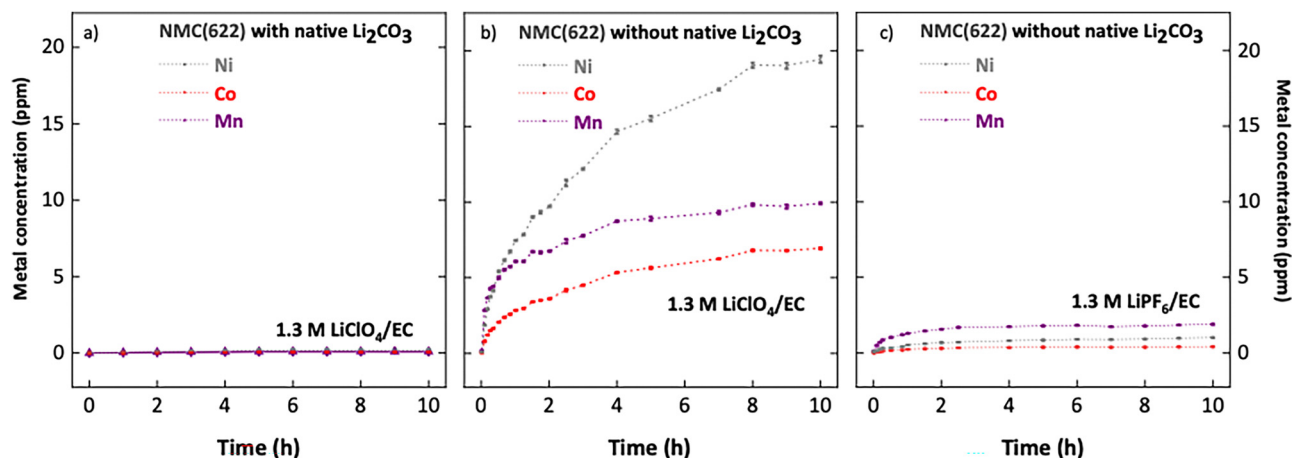This journal is © The Royal Society of Chemistry 2025

Fig. 7 Measurements of Ni, Co and Mn ICP-MS collected at different time intervals after exposing 100 mg of the unwashed NMC622 sample to 5 mL of the electrolyte containing 3 mM of protons for the 1.3 M LiClO$_4$/EC electrolyte (a), 30 mg of the washed NMC622 sample to 3 mL of the electrolyte containing 3 mM of protons for the 1.3 M LiClO$_4$/EC electrolyte (b) and 1.3 M LiPF$_6$/EC electrolyte (c). The standard deviation for each point is shown as an error bar.

consumption of protons. We also verified the existence of quantitative reactions by the absence of the characteristic H$^+$/H$_2$ feature at 3.2 V *vs.* Li/Li$^+$ in the cyclic voltammogram on Pt electrodes performed in oxidized electrolytes after exposure to NMC powder (Fig. S11, ESI†). However, compared to the expected stoichiometric Ni : Mn : Co ratio of 6 : 2 : 2, we observe a somewhat skewed 6 : 3 : 2 ratio, suggesting a preferential dissolution of Mn from NMC, consistent with the literature of cathode corrosion. This skew is even more evident when the oxidized electrolyte is 1.3 M LiPF$_6$/EC, where the Ni : Mn : Co ratio was 2 : 4 : 1, again favouring Mn. Nonetheless, the quenching of H$^+$ by PF$_6^-$ made the dissolution rate 10 times lower than that by LiClO$_4$. Thus, under these conditions, the NMC powder can react both with protons and with HF formed *via* reaction (2). Many have suggested that the presence of HF is particularly detrimental to Mn,[74–77] which would be consistent with our observations. Our results emphasize that the protons generated from electrolyte oxidation are not as selective as HF. We further speculate that greater degrees of dissolution of NMC could also be impeded by the formation of a passive film on NMC containing other fluorinated byproducts, such as lithium and transition metal fluorides, which have been observed on cathode surfaces after degradation.[78–80]

2.6 Assessment of impact on battery performance

Finally, we aimed to evaluate the effect of the activity of H$^+$ on the performance of full graphite∥NMC622 cells. For this purpose, we used 1.3 M LiClO$_4$ in EC/EMC mixtures to approach the compositions of conventional electrolytes while still highlighting the role of H$^+$ by avoiding their secondary reactions with LiPF$_6$. We compared the pristine electrolyte with a sample that was subjected to oxidation on Pt(111). We also envisaged a clean way of introducing H$^+$ without other confounding compounds associated with electrolyte degradation at very high potential by performing electrochemical oxidation of H$_2$ gas (HOR) bubbled through the electrolyte using a Pt(111)

electrode, a process that can be conducted at much lower potentials than electrolyte oxidation. The performance of full cells with these three types of electrolytes (pristine, electrochemically oxidized and with H$^+$ added *via* HOR) is compared in Fig. 8. It is immediately apparent that the introduction of H$^+$, by either the HOR or solvent electro-oxidation, has a destructive effect on the battery performance as its presence is associated with higher overpotential and a nontrivial capacity drops, even when cycling at relatively mild potentials (4.2–2.7 V). The negative impact of electrochemically generated protons can also be seen in the case of a state-of-the-art Li-ion electrolyte (1 M LiPF$_6$/EC/EMC + 2%VC), where even introduction of small amounts of protons (3 mM) *via* the HOR is sufficient to degrade electrolyte performance upon storage when used in the same full cell configuration (Fig. S12, ESI†), highlighting their catalytic activity. It is worth noting that even higher concentrations of H$^+$ than we were able introduce in the bulk electrolyte could be locally achieved at cathode–electrolyte interfaces when
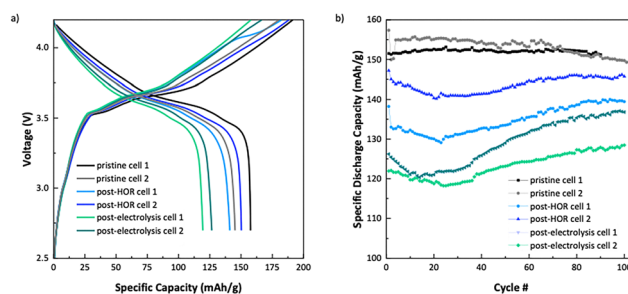

Fig. 8 Effect of protons on the battery performance using 1.3 M LiClO$_4$ in EC/EMC electrolytes and NMC622/Graphite 2032-coin cells, where ∼3 mM of protons were introduced either *via* electrochemical oxidation of H$_2$ (post-HOR) or by electrochemical oxidation of the electrolyte (post-electrolysis): (a) charge/discharge curve of the first cycle and (b) long-term cycling performance of cells performed at C/10 for three charge/discharge cycles before long-term cycling at C/3 (1C = 1.41 mA cm^{-2}). All cells were tested with a cutoff voltage of 4.2–2.7 V.

This journal is © The Royal Society of Chemistry 2025

Energy Environ. Sci., 2025, **18**, 8303–8312 | **8309**

their generation occurs simultaneous to battery operation under harsher upper voltages, meaning that even small parasitic currents of solvent oxidation can be behind observable macroscopic consequences. Moreover, the proton formation upon solvent oxidation occurs in other commercial carbonate-based solvents, additives and even impurities (Fig. S13, ESI†), which further emphasizes the need for their remediation.

3. Conclusions

In summary, we establish that $LiClO_4$/EC and $LiPF_6$/EC based electrolytes, common in Li-ion batteries, start decomposing to form highly reactive protons above 4.0 V *vs.* Li^+/Li^0, values that are relevant for the operation of high-voltage Li-ion batteries. The solvent oxidation takes place even in the absence of oxide surfaces, and is prevalent on carbon, which is always a component of cathode composites. The chemical properties of the electrogenerated protons were found to be comparable with those of known superacids. Once formed, these protons trigger additional bulk and interfacial degradation *via* a cascade of chemical reactions even under open circuit conditions or during electrolyte storage, and which include products mistakenly ascribed to the electrochemical process. Indeed, protons thermally catalyse further decomposition of intact EC, forming CO_2 and ethers that quite possibly include PEO fragments, and promote dissolution of transition metals from prototypical NMC active materials. Electrolytes based on $LiPF_6$ open another chemical pathway *via* the quantitative formation of the weaker acid HF, which then proceeds to trigger its own degradation mechanisms. Our results indicate that the generation of protons under these conditions must be avoided at all costs. While it could be argued that some mitigation is unwittingly provided by the fluorinated salt in the electrolyte and/or carbonate impurities on cathode surfaces, this activity does not provide a sustainable path because it only triggers other sources of degradation that battery engineers seek to avoid. Most importantly, the slow reaction rates mean that these chemically aggressive protons have ample time to degrade essentially all battery components, particularly the solvent, before being consumed. Therefore, a sustainable strategy remains to be identified to avoid or, at least, mitigate proton abstraction due to the electrochemical oxidation of battery electrolytes. Our work reveals a key route to long-term degradation that should inform efforts to design battery components that enable vertical leaps in performance for high-energy density batteries.

Author contributions

S. I., M. M., H. L., J. G. C., B. K., J. C., and D. S. helped with the conception of this manuscript. S. I. T. H. and M. M. performed electrochemical experiments in flooded cells and analysis, and P. F. B. D. M. and D. H. performed OEMS experiments. H. L. and B. K. performed NMR experiments. S. E. W. and L. F. W. performed the DFT evaluations and analysis of the electrochemical reaction mechanism. B. G. performed the analysis of chemical reaction mechanisms. J. Y. and Z. Z. performed the battery discharge experiments and analysis. S. I., M. M., J. C., and D. S. analyzed crucial data and wrote the manuscript.

Conflicts of interest

There are no conflicts to declare.

Data availability

All data supporting the findings of this study are included in the manuscript and the ESI,† or are available from the corresponding author upon reasonable request.

Acknowledgements

References

1 J. W. Choi and D. Aurbach, *Nat. Rev. Mater.*, 2016, **1**, 16013.
2 K. Xu, *Chem. Rev.*, 2014, **114**, 11503–11618.
3 V. Etacheri, R. Marom, R. Elazari, G. Salitra and D. Aurbach, *Energy Environ. Sci.*, 2011, **4**, 3243.
4 W. Li, B. Song and A. Manthiram, *Chem. Soc. Rev.*, 2017, **46**, 3006–3059.
5 X. Fan and C. Wang, *Chem. Soc. Rev.*, 2021, **50**, 10486–10566.
6 H. Wan, J. Xu and C. Wang, *Nat. Rev. Chem.*, 2023, **8**, 30–44.
7 K. Xu, *Chem. Rev.*, 2004, **104**, 4303–4418.
8 J. Xiang, Y. Wei, Y. Zhong, Y. Yang, H. Cheng, L. Yuan, H. Xu and Y. Huang, *Adv. Mater.*, 2022, **34**, 2200912.
9 A. Manthiram, *Nat. Commun.*, 2020, **11**, 1550.
10 N. Membreño, K. Park, J. B. Goodenough and K. J. Stevenson, *Chem. Mater.*, 2015, **27**, 3332–3340.
11 S. Ko, Y. Yamada and A. Yamada, *Joule*, 2021, **5**, 998–1009.
12 Y.-K. Sun, S.-T. Myung, M.-H. Kim, J. Prakash and K. Amine, *J. Am. Chem. Soc.*, 2005, **127**, 13411–13418.
13 Y.-K. Sun, Z. Chen, H.-J. Noh, D.-J. Lee, H.-G. Jung, Y. Ren, S. Wang, C. S. Yoon, S.-T. Myung and K. Amine, *Nat. Mater.*, 2012, **11**, 942–947.
14 D. Aurbach, B. Markovsky, G. Salitra, E. Markevich, Y. Talyossef, M. Koltypin, L. Nazar, B. Ellis and D. Kovacheva, *J. Power Sources*, 2007, **165**, 491–499.

8310 | *Energy Environ. Sci.*, 2025, **18**, 8303–8312

This journal is © The Royal Society of Chemistry 2025

15 S. Solchenbach, G. Hong, A. T. S. Freiberg, R. Jung and H. A. Gasteiger, *J. Electrochem. Soc.*, 2018, **165**, A3304–A3312.

16 F. Lin, I. M. Markus, D. Nordlund, T.-C. Weng, M. D. Asta, H. L. Xin and M. M. Doeff, *Nat. Commun.*, 2014, **5**, 3529.

17 S. Jung, H. Gwon, J. Hong, K. Park, D. Seo, H. Kim, J. Hyun, W. Yang and K. Kang, *Adv. Energy Mater.*, 2014, **4**, 1300787.

18 W. Li, A. Dolocan, P. Oh, H. Celio, S. Park, J. Cho and A. Manthiram, *Nat. Commun.*, 2017, **8**, 14589.

19 J. C. Hestenes, J. T. Sadowski, R. May and L. E. Marbella, *ACS Mater. Au*, 2023, **3**, 88–101.

20 H. Y. Asl and A. Manthiram, *Science*, 2020, **369**, 140–141.

21 W. Choi and A. Manthiram, *J. Electrochem. Soc.*, 2006, **153**, A1760.

22 Z. Zhang, S. Said, A. J. Lovett, R. Jervis, P. R. Shearing, D. J. L. Brett and T. S. Miller, *ACS Nano*, 2024, **18**, 9389–9402.

23 M. Jiang, D. L. Danilov, R. Eichel and P. H. L. Notten, *Adv. Energy Mater.*, 2021, **11**, 2103005.

24 O. Borodin, X. Ren, J. Vatamanu, A. Von Wald Cresce, J. Knap and K. Xu, *Acc. Chem. Res.*, 2017, **50**, 2886–2894.

25 P. Peljo and H. H. Girault, *Energy Environ. Sci.*, 2018, **11**, 2306–2309.

26 J. L. Tebbe, T. F. Fuerst and C. B. Musgrave, *ACS Appl. Mater. Interfaces*, 2016, **8**, 26664–26674.

27 N. Kumar, K. Leung and D. J. Siegel, *J. Electrochem. Soc.*, 2014, **161**, E3059–E3065.

28 S. Xu, G. Luo, R. Jacobs, S. Fang, M. K. Mahanthappa, R. J. Hamers and D. Morgan, *ACS Appl. Mater. Interfaces*, 2017, **9**, 20545–20553.

29 K. Leung, *J. Phys. Chem. C*, 2012, **116**, 9852–9861.

30 J. Han, K. Kim, Y. Lee and N. Choi, *Adv. Mater.*, 2019, **31**, 1804822.

31 S. E. Sloop, J. B. Kerr and K. Kinoshita, *J. Power Sources*, 2003, **119–121**, 330–337.

32 Y. Zhang, Y. Katayama, R. Tatara, L. Giordano, Y. Yu, D. Fraggedakis, J. G. Sun, F. Maglia, R. Jung, M. Z. Bazant and Y. Shao-Horn, *Energy Environ. Sci.*, 2020, **13**, 183–199.

33 B. L. D. Rinkel, J. P. Vivek, N. Garcia-Araez and C. P. Grey, *Energy Environ. Sci.*, 2022, **15**, 3416–3438.

34 E. W. C. Spotte-Smith, S. Vijay, T. B. Petrocelli, B. L. D. Rinkel, B. D. McCloskey and K. A. Persson, *J. Phys. Chem. Lett.*, 2024, **15**, 391–400.

35 A. T. S. Freiberg, M. K. Roos, J. Wandt, R. De Vivie-Riedle and H. A. Gasteiger, *J. Phys. Chem. A*, 2018, **122**, 8828–8839.

36 M. H. V. Huynh and T. J. Meyer, *Chem. Rev.*, 2007, **107**, 5004–5064.

37 J.-F. Zhi, H.-B. Wang, T. Nakashima, T. N. Rao and A. Fujishima, *J. Phys. Chem. B*, 2003, **107**, 13389–13395.

38 M. T. M. Koper, S. C. S. Lai and E. Herrero, in *Fuel Cell Catalysis*, ed. M. T. M. Koper, Wiley, 1st edn, 2009, pp. 159–207.

39 T. Hatsukade, M. Zorko, D. Haering, N. M. Markovic, V. R. Stamenkovic and D. Strmcnik, *Electrochem. Commun.*, 2020, **120**, 106785.

40 W. Yin, S. Mariyappan, A. Grimaud and J. M. Tarascon, *J. Electrochem. Soc.*, 2018, **165**, A3326–A3333.

41 R. Jung, M. Metzger, F. Maglia, C. Stinner and H. A. Gasteiger, *J. Phys. Chem. Lett.*, 2017, **8**, 4820–4825.

42 M. Metzger, C. Marino, J. Sicklinger, D. Haering and H. A. Gasteiger, *J. Electrochem. Soc.*, 2015, **162**, A1123–A1134.

43 L. A. Kaufman and B. D. McCloskey, *Chem. Mater.*, 2021, **33**, 4170–4176.

44 Charles J. Pouchert, *The Aldrich library of NMR spectra*, Aldrich Chemical Co., Milwaukee, Wis. (P.O. Box 355, Milwaukee 53201), 1983, vol. 1 & 2.

45 J. F. Haw, J. B. Nicholas, T. Xu, L. W. Beck and D. B. Ferguson, *Acc. Chem. Res.*, 1996, **29**, 259–267.

46 G. E. Salnikov, A. M. Genaev, V. G. Vasiliev and V. G. Shubin, *Org. Biomol. Chem.*, 2012, **10**, 2282.

47 T. Birchall and R. J. Gillespie, *Can. J. Chem.*, 1964, **42**, 502–513.

48 J.-C. Culmann, M. Fauconet, R. Jost and J. Sommer, *New J. Chem.*, 1999, **23**, 863–867.

49 M. Juhasz, S. Hoffmann, E. Stoyanov, K. Kim and C. A. Reed, *Angew. Chem., Int. Ed.*, 2004, **43**, 5352–5355.

50 M. J. Crafton, T.-Y. Huang, Z. Cai, Z. M. Konz, N. Guo, W. Tong, G. Ceder and B. D. McCloskey, *J. Electrochem. Soc.*, 2024, **171**, 020530.

51 S. E. Sloop, J. B. Kerr and K. Kinoshita, *J. Power Sources*, 2003, **119–121**, 330–337.

52 L. Yang, B. Ravdel and B. L. Lucht, *Electrochem. Solid-State Lett.*, 2010, **13**, A95.

53 O. Borodin, W. Behl and T. R. Jow, *J. Phys. Chem. C*, 2013, **117**, 8661–8682.

54 K. Leung, *J. Phys. Chem. C*, 2013, **117**, 1539–1547.

55 O. Borodin, M. Olguin, C. E. Spear, K. W. Leiter and J. Knap, *Nanotechnology*, 2015, **26**, 354003.

56 O. Borodin, X. Ren, J. Vatamanu, A. Von Wald Cresce, J. Knap and K. Xu, *Acc. Chem. Res.*, 2017, **50**, 2886–2894.

57 S. Xu, G. Luo, R. Jacobs, S. Fang, M. K. Mahanthappa, R. J. Hamers and D. Morgan, *ACS Appl. Mater. Interfaces*, 2017, **9**, 20545–20553.

58 D. Chen, M. A. Mahmoud, J.-H. Wang, G. H. Waller, B. Zhao, C. Qu, M. A. El-Sayed and M. Liu, *Nano Lett.*, 2019, **19**, 2037–2043.

59 Y. Jin, N.-J. H. Kneusels and C. P. Grey, *J. Phys. Chem. Lett.*, 2019, **10**, 6345–6350.

60 B. L. D. Rinkel, D. S. Hall, I. Temprano and C. P. Grey, *J. Am. Chem. Soc.*, 2020, **142**, 15058–15074.

61 E. Castel, E. J. Berg, M. El Kazzi, P. Novák and C. Villevieille, *Chem. Mater.*, 2014, **26**, 5051–5057.

62 M. Arakawa and J. Yamaki, *J. Power Sources*, 1995, **54**, 250–254.

63 D. Streich, C. Erk, A. Guéguen, P. Müller, F.-F. Chesneau and E. J. Berg, *J. Phys. Chem. C*, 2017, **121**, 13481–13486.

64 L. Xing and O. Borodin, *Phys. Chem. Chem. Phys.*, 2012, **14**, 12838.

65 W. M. Dose, W. Li, I. Temprano, C. A. O'Keefe, B. L. Mehdi, M. F. L. De Volder and C. P. Grey, *ACS Energy Lett.*, 2022, **7**, 3524–3530.

66 R. Abdul-Karim, A. Hameed and M. I. Malik, *RSC Adv.*, 2017, **7**, 11786–11795.

This journal is © The Royal Society of Chemistry 2025

Energy Environ. Sci., 2025, **18**, 8303–8312 | 8311

67 J. Cabana, B. J. Kwon and L. Hu, *Acc. Chem. Res.*, 2018, **51**, 299–308.

68 D. Strmcnik, I. E. Castelli, J. G. Connell, D. Haering, M. Zorko, P. Martins, P. P. Lopes, B. Genorio, T. Østergaard, H. A. Gasteiger, F. Maglia, B. K. Antonopoulos, V. R. Stamenkovic, J. Rossmeisl and N. M. Markovic, *Nat. Catal.*, 2018, **1**, 255–262.

69 M. Liu, J. Vatamanu, X. Chen, L. Xing, K. Xu and W. Li, *ACS Energy Lett.*, 2021, **6**, 2096–2102.

70 J. S. Edge, S. O'Kane, R. Prosser, N. D. Kirkaldy, A. N. Patel, A. Hales, A. Ghosh, W. Ai, J. Chen, J. Yang, S. Li, M.-C. Pang, L. Bravo Diaz, A. Tomaszewska, M. W. Marzook, K. N. Radhakrishnan, H. Wang, Y. Patel, B. Wu and G. J. Offer, *Phys. Chem. Chem. Phys.*, 2021, **23**, 8200–8221.

71 W. Liu, P. Oh, X. Liu, M. Lee, W. Cho, S. Chae, Y. Kim and J. Cho, *Angew. Chem., Int. Ed.*, 2015, **54**, 4440–4457.

72 D.-H. Cho, C.-H. Jo, W. Cho, Y.-J. Kim, H. Yashiro, Y.-K. Sun and S.-T. Myung, *J. Electrochem. Soc.*, 2014, **161**, A920–A926.

73 G. V. Zhuang, G. Chen, J. Shim, X. Song, P. N. Ross and T. J. Richardson, *J. Power Sources*, 2004, **134**, 293–297.

74 J. C. Hestenes, J. T. Sadowski, R. May and L. E. Marbella, *ACS Mater. Au*, 2023, **3**, 88–101.

75 H. Y. Asl and A. Manthiram, *Science*, 2020, **369**, 140–141.

76 W. Choi and A. Manthiram, *J. Electrochem. Soc.*, 2006, **153**, A1760.

77 C. Wang, L. Xing, J. Vatamanu, Z. Chen, G. Lan, W. Li and K. Xu, *Nat. Commun.*, 2019, **10**, 3423.

78 Q. Zhang, J. Ma, L. Mei, J. Liu, Z. Li, J. Li and Z. Zeng, *Matter*, 2022, **5**, 1235–1250.

79 D. Aurbach, K. Gamolsky, B. Markovsky, G. Salitra, Y. Gofer, U. Heider, R. Oesten and M. Schmidt, *J. Electrochem. Soc.*, 2000, **147**, 1322.

80 S. K. Martha, E. Markevich, V. Burgel, G. Salitra, E. Zinigrad, B. Markovsky, H. Sclar, Z. Pramovich, O. Heik, D. Aurbach, I. Exnar, H. Buqa, T. Drezen, G. Semrau, M. Schmidt, D. Kovacheva and N. Saliyski, *J. Power Sources*, 2009, **189**, 288–296.

8312 | *Energy Environ. Sci.*, 2025, **18**, 8303–8312

This journal is © The Royal Society of Chemistry 2025